Unsteady flow and mass transfer in models of stenotic arteries considering fluid-structure interaction☆

Alvaro Valencia *, Martin Villanueva

Department of Mechanical Engineering, Universidad de Chile, Casilla 2777, Santiago, Chile

Abstract

In this work the unsteady non-Newtonian blood flow and mass transfer in symmetric and non-symmetric stenotic arteries are numerically simulated considering the fluid-structure interaction (FSI) using the code ADINA. Blood with hyperviscosity syndrome is considered and hyperelastic Mooney–Rivlin model is used for the compliant arterial wall. The inlet boundary condition of imposed velocity or pressure is critical to obtain realistic hemodynamic results in stenotic arteries. The FSI affects significantly the hemodynamics on the stenotic arteries models, the arteries are considerably dilated and compressed due the stenosis. The stenosis severity and geometry have important influence on recirculation length, and distribution of concentration of macromolecules, such as low density lipoproteins (LDL).

Keywords: CFD; FSI; Stenosis; Blood flow; Artery compression; Artery dilatation

1. Introduction

Flow through severely atherosclerotic arteries is of great interest. These arteries pose grave health risks and are a major cause of mortality and morbidity in the industrialized world. Narrowing of an artery, or stenosis, can result from substantial plaque deposit, and may cause a severe reduction of blood flow. The plaque may also break off into particles, or emboli, which may lodge in an artery downstream. In cerebral arteries the danger of embolism is that the ruptured particles are carried into the brain, provoking neurological symptoms or a stroke. The difficulties in making realistic experimental and numerical investigations of the blood flow in stenotic arteries are the non-Newtonian rheology of blood, the compliant characteristic of arterial wall, the pulsatile inlet flow, the mass transfer, the geometry of the stenosis, and the transition to turbulent flow. These issues have been partially addressed in recent studies investigating flow through stenotic arteries.

The flow in a stenotic artery is characterized by high pressure and WSS at the throat and a recirculation zone observed distal to the stenosis. The recirculation zone varies during one cardiac pulse and the recirculation length depends on stenosis severity, stenosis morphology, Reynolds number, and Womersley number of the pulsatile flow,

☆ Communicated by W.J. Minkowycz.

* Corresponding author.
E-mail address: alvalenc@ing.uchile.cl (A. Valencia).

Nomenclature

ALE	Lagrangian–Eulerian
a	Cerebral artery diameter
c_1, c_2, D_1, D_2	Mooney–Rivlin material constants
d_I	Displacement
D	Diffusivity of LDL
FSI	Fluid-structure interaction
h	Arterial thickness
LDL	Low density lipoproteins
Lr	Recirculation length
M–R	Mooney–Rivlin model
p	Pressure
S	Stenosis severity based on diameter reduction
u	Velocity
U	Mean velocity at inlet
W	Strain energy
WSS	Wall shear stress

Greek symbols

λ	Stretch ratio
μ	Viscosity
ρ	Density
σ	Stress
τ	Shear stress
Φ	Mass ratio

[1,2]. The phenomenon of periodic shedding of vortices downstream of the stenotic throat, on axisymmetric stenosis with an area reduction of 84%, begins at approximately Reynolds number of $Re=375$, [3].

Bathe and Kamm [4] conducted a finite element analysis to examine the FSI of pulsatile flow through a compliant stenotic artery. They use the commercial software ADINA to develop an axisymmetric model of the flow and vessel. They observed an increase in the pressure drop and wall shear stress associated with the flow as they increased the stenosis severity. They also reported an increase in the inner hoop stretch and compressive stresses on the lesion, as well as additional decreases in vessel area during peak systolic time. Tang et al. [5] also considered FSI of unsteady flow through a stenotic vessel. They observed complex flow patterns and high shear stresses at the throat of the stenosis, as well as cyclic tube compression. Tang et al. [6] studied the FSI on stenotic arterial models with lipid pool using the software ADINA. The results indicate that critical plaque stress/strain conditions are affected by stenosis severity, stenosis eccentricity, lipid pool size, plaque cap thickness, and initial arterial stretch. Three-dimensional MRI-based computational models of stenotic arteries were studied also by Tang et al. [7]. The results indicate that large lipid pools and thin plaque caps are associated with maximum stretch and minimum compression stress levels. The compliant arterial wall, which must withstand arterial blood pressure, is composed of layered collagen. Wall strength is related to both collagen fiber strength and orientation. Fluid shear stress modulates endothelial cell remodeling via realignment and elongation, and the time variation of WSS affects significantly the rates at which endothelial cells remodel [8].

In large arteries with severe stenosis turbulent flow patterns appear in the post-stenotic area for upstream Reynolds numbers $Re>500$. Both steady and pulsatile simulations of turbulent flow were carried out by Stroud et al. [9] in the examination of a severely stenosed two-dimensional model. The model was based on a single slice of a high-resolution image of an anatomical carotid plaque obtained after carotid endarterectomy surgery. The flow distal the stenosis was likely transitional, so a model that captured both laminar and turbulent flow regimes for the different phases of pulsatile flow was required. Varghese and Frankel [10] investigated pulsatile turbulent flow in stenotic vessels using the

Reynolds-averaged Navier–Strokes approach. All models predicted a WSS peak at the throat of the stenosis with minimum values observed distal to the stenosis where flow separation occurred.

The transport of macromolecules, such as LDL across the artery wall is a key step in atherogenesis. Stangeby and Ethier [11] reported the fluid flow and mass transfer of LDL in a stenotic artery, the results show an elevated LDL concentration at the downstream side of the stenosis. The mass transport on symmetric and non-symmetric stenotic artery models was studied in Ref. [12]. The complex flow field due to the non-symmetric stenosis resulted in mass transfer patterns substantially different than those exhibited by the symmetric stenosis.

This paper presents detailed numerical simulations of the unsteady laminar non-Newtonian fluid flow and mass transfer of LDL macromolecules in symmetric and non-symmetric stenotic cerebral arteries models. Blood with hyperviscosity syndrome is considered to simulate macroglobulinemia condition, [13]. The effects of compliant arterial wall are considered with imposed inlet pressure for four stenosis severities, and the results are compared with those of models with rigid walls and imposed inlet velocity.

2. Mathematical and numerical modeling

2.1. Fluid and solid models

For the fluid model, the flow was assumed to be laminar, non-Newtonian, and incompressible. The incompressible Navier–Stokes equations with arbitrary ALE formulation were used as the governing equations which are suitable for problems with FSI and frequent mesh adjustments. Flow velocity at the flow–artery interface was set to move with the artery wall.

Continuity:

$$\nabla \cdot \mathbf{u} = 0 \tag{1}$$

Equation of Navier–Stokes:

$$\rho_f(\partial \mathbf{u}/\partial t + ((\mathbf{u}-\mathbf{u}_g)\cdot\nabla)\mathbf{u}) = -\nabla p + \nabla \cdot \tau \tag{2}$$

Mass transfer:

$$\partial \phi/\partial t + \nabla \cdot(\mathbf{u}\phi) = D\nabla^2\phi \tag{3}$$

where ρ_f is the fluid density, $\mathbf{u}$ is the fluid velocity vector and $\mathbf{u}_g$ is the moving coordinate velocity, respectively. In the ALE formulation, $(\mathbf{u}-\mathbf{u}_g)$ is the relative velocity of the fluid with respect to the moving coordinate velocity, and τ is the deviatoric stress tensor. Blood is modeled to have a density $\rho_f = 1050$ kg/m^3.

The blood is a non-Newtonian fluid. Blood with hyperviscosity syndrome is considered in this investigation to simulate blood flow under macroglobulinemia condition, in this case the blood viscosity depends on the hematocrit as well on the macroglobulin concentration, [13]. The Carreau non-Newtonian model can be used to describe the variation of normal blood viscosity with the shear rate. The Carreau model assumes that the viscosity ì varies according to the law

$$\mu = \mu_\infty + (\mu_0-\mu_\infty)[1 + (\lambda\,\boldsymbol{\gamma})^2]^{(n-1)/2} \tag{4}$$

where $\lambda = 3.313$ s, $n = 0.3568$, $\mu_0 = 0.056$ kg/ms and $\mu_\infty = 0.00345$ kg/ms, [14]. This normal viscosity of blood was multiplied by a factor 10 to simulate the hyperviscosity syndrome condition of diseases in the blood.

The transport of LDL is governed by Eq. (3), where Φ is the mass ratio between LDL concentration and blood density, the diffusivity of LDL in blood is $D = 5\times10^{-12}$ m^2/s, [11]. The mass transfer boundary conditions were as follows: a uniform mass ratio $\Phi = 0.0011$ was imposed at the inlet, [11], a Dirichlet boundary condition of $\Phi = 0$ was set on the arterial walls, and a zero gradient was applied at the outlet. Setting $\Phi = 0$ on arterial walls is appropriate in this case, because convective effects dominate LDL transport in the arterial walls, [11].

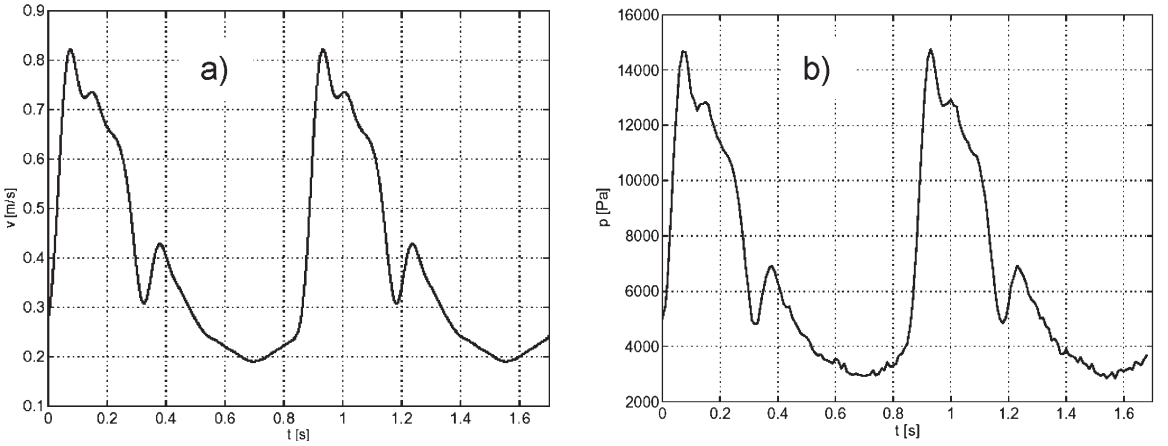

Fig. 1. a) Time dependent velocity at inlet, b) Time dependent pressure at inlet.

The governing equation for the solid domain is the momentum conservation equation given by Eq. (5). In contrast to the ALE formulation of the fluid equations, a Lagrangian coordinate system is adopted:

$$\nabla \boldsymbol{\sigma}_s = \rho_s \ddot{d}_s \tag{5}$$

where ρ_S is the solid density, $\boldsymbol{\sigma}_S$ is the solid stress tensor, and $\ddot{d}_s$ is the local acceleration of the solid. The artery wall was assumed to be hyperelastic, isotropic, incompressible, and homogeneous with a density $\rho_S = 1050$ kg/m^3. The applied boundary conditions on the fluid domain are: (i) a time dependent velocity at inlet in the models with rigid walls or a time dependent pressure in the FSI models, and (ii) a zero normal traction at outlet. These are presented in mathematical form in Eqs. (6) and (7):

$$u|_{\text{inlet}} = U(t) \quad or \quad \sigma_{nn}|_{\text{inlet}} = P(t) \tag{6}$$

$$\sigma_{nn}|_{\text{outlet}} = 0 \tag{7}$$

Physiologically flow condition is imposed using flow measurements with pulsed Doppler ultrasound acquired in the right internal carotid artery for a patient with a stenosis of 80% based on diameter reduction. The heart rate is 70 bpm. The mean blood velocity is 39.8 cm/s. The time dependence of the inflow mean velocity $U(t)$ is shown in Fig. 1a. Peak systolic flow occurs at $t = 0.075$ s. For the simulations with FSI a pressure boundary condition is imposed at inlet, because the artery upstream the stenosis exhibits important dilatation. If the velocity boundary condition is used, the blood flow will be

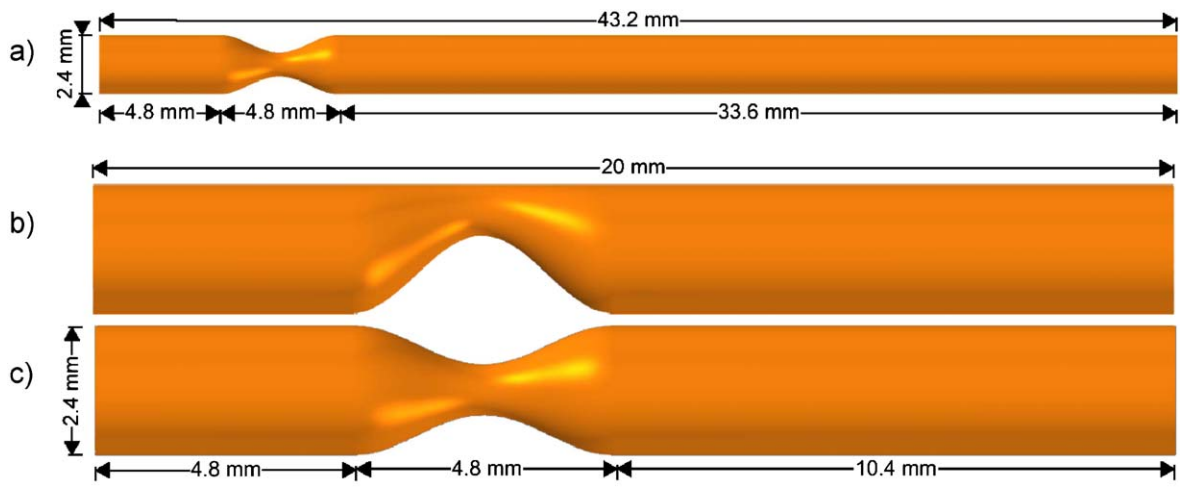

Fig. 2. Models geometry: a) symmetric stenotic artery with rigid walls, b) non-symmetric stenotic artery with FSI, c) symmetric stenotic artery with FSI. $S = 60\%$.

Table 1
Mesh refinement comparisons at systolic time 0.932 s for the mean velocity at throat, S=66%, artery volume 185.3 mm^3

Symmetric rigid artery			Non-symmetric rigid artery		
Elements	[elem./mm^3]	v [m/s]	Elements	[elem./mm^3]	v [m/s]
8320	44.89	5.91	15439	83.31	4.30
16000	86.33	6.00	31372	169.29	4.47
36000	194.25	6.53	70682	381.43	4.72
48334	260.80	6.43	134003	723.13	4.70

artificially increased. The cases with rigid wall are first simulated, and the variation of pressure with the time $P(t)$ at inlet in one cardiac cycle for the case with S=50% is imposed as inlet boundary condition for the 8 FSI simulations, see Fig. 1b. The effects of exit pressure boundary conditions on the flow in a carotid bifurcation were investigated in [15]. The boundary conditions on the FSI interfaces state that: (i) displacements of the fluid and solid domain must be compatible, (ii) tractions at these boundaries must be at equilibrium and (iii) fluid obeys the no-slip condition. These conditions are given in Eqs. (8), (9) and (10):

$$\mathbf{d}_s = \mathbf{d}_f \tag{8}$$

$$\boldsymbol{\sigma}_s \cdot \hat{n}_s = \boldsymbol{\sigma}_f \cdot \hat{n}_f \tag{9}$$

$$\dot{\mathbf{d}}_s = \dot{\mathbf{d}}_f \tag{10}$$

where $\mathbf{d}$, σ and $\hat{n}$ are displacements, stress tensors and boundary normals with the subscripts f and s indicating a property of the fluid and solid, respectively. The 3D hyperelastic M–R model was used to describe the material properties of the artery wall, [7]. The strain energy function is given in the M–R model by:

$$W = c_1(I_1-3) + c_2(I_2-3) + D_1[\exp(D_2(I_1-3))-1] \tag{11}$$

$$I_1 = C_{kk} \qquad I_2 = 1/2[{I_1}^2 - C_{ij}C_{ij}] \tag{12}$$

where I_1 and I_2 are the first and second strain invariants of the Cauchy–Green deformation tensor, c_1, c_2, D_1 and D_2 are material constants, [16]. Assuming:

$$\lambda_1\lambda_2\lambda_3 = 1, \quad \lambda_2 = \lambda_3, \quad \lambda = \lambda_1 \tag{13}$$

where λ_1, λ_2, and λ_3 are stretch ratios in (x,y,z) directions respectively, the uniaxial stress/stretch relation for an isotropic material is obtained from Eq. (11)

$$\sigma = \partial W/\partial\lambda = c_1[2\lambda - 2\lambda^{-2}] + c_2[2 - 2\lambda^{-3}] + D_1D_2[2\lambda - 2\lambda^{-2}]\exp[D_2(\lambda^2 + 2/\lambda - 3)] \tag{14}$$

In this work, the following values were chosen to match the M–R uniaxial stress/stretch relation with experimental data for a normal artery, c_1=9200. Pa, c_2=0, D_1=3600. Pa and D_2=2.0, [7]. With these values the M–R model fits average uniaxial

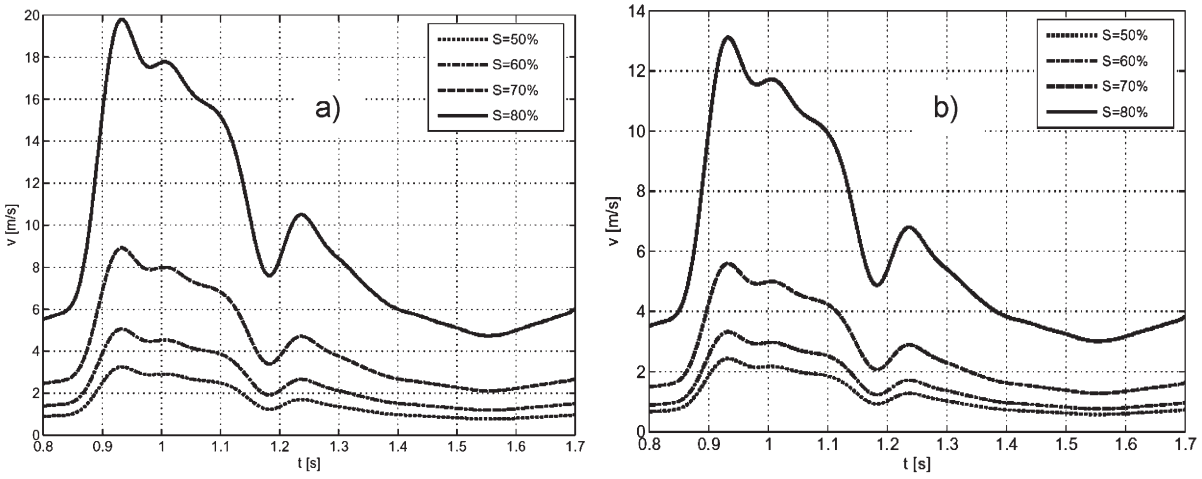

Fig. 3. Mean velocity at throat versus time with rigid walls: a) symmetric stenotic arteries, b) non-symmetric stenotic arteries.

Table 2
Maximal pressure (located at inlet) and minimal pressure (located at throat) for systolic time 0.932 s with rigid walls

	P max [Pa]		*P* min [Pa]	
S [%]	Sym	Non-sym	Sym	Non-sym
50	14,793.	16,757.	0	0
60	26,850.	29,081.	−3415.	0
70	72,709.	73,068.	−17,293.	−10,733.
80	350,061.	331,244.	−73,321.	−68,788.

behavior of normal arteries stretched in the experiments. Arteries shrink about 30% to 50% when removed from *in vivo* condition. For this reason, in this paper the eight cases with FSI have initial axial stretch of the artery of 36.5%, [6], to obtain realistic artery stress and stretch under physiological pulsatile inlet blood pressure. Fig. 2 shows the domain for the cases with rigid walls and the cases with FSI. Cases with rigid arterial wall or FSI for symmetric and non-symmetric stenosis were investigated for $S=50\%$, 60%, 70% and 80%. The geometry of the stenosis was obtained from [5]. The displacements are restricted after the stretching in the axial direction. These restrictions are applied far from the stenosis, and therefore they do not affect the deformation and effective stress in the wall artery near the stenosis. The arterial wall has a thickness of 0.24 mm, and it is simulated as 3D solid wall.

2.2. Numerical method

The fully coupled fluid and structure models were solved by a commercial finite element package ADINA (v8.2, ADINA R and D, Inc., Cambridge, MA) which has been tested by several applications, [16]. The Finite Element Method (FEM) is used to solve the governing equations. The FEM discretizes the computational domain into finite elements that are interconnected by element nodal points. The fluid domain employs special Flow-Condition-Based-Interpolation (FCBI) tetrahedral elements, [16]. We have used the formulation with large displacements and small strains in the FSI calculation available in ADINA. As iteration we used full Newton method with a maximum of 80 iterations in each time step of 0.002 s. A sparse matrix solver based on Gaussian elimination is used for solving the system. The relative tolerance for all degrees of freedom was set to 0.01.

Structured grids composed of eight-node hexahedral elements were used in the fluid only in the 4 cases with rigid wall and symmetric stenosis. Unstructured grids were used in the other investigated cases. The unstructured grids were composed of tetrahedral with four-node elements in the fluid and hexahedral with eight-node elements in the solid. To verify grid independence, numerical simulations based on symmetric and asymmetric stenosis with $S=66\%$ and with rigid walls were performed for four grids sizes. Table 1 shows the convergence of mean velocity at throat for the

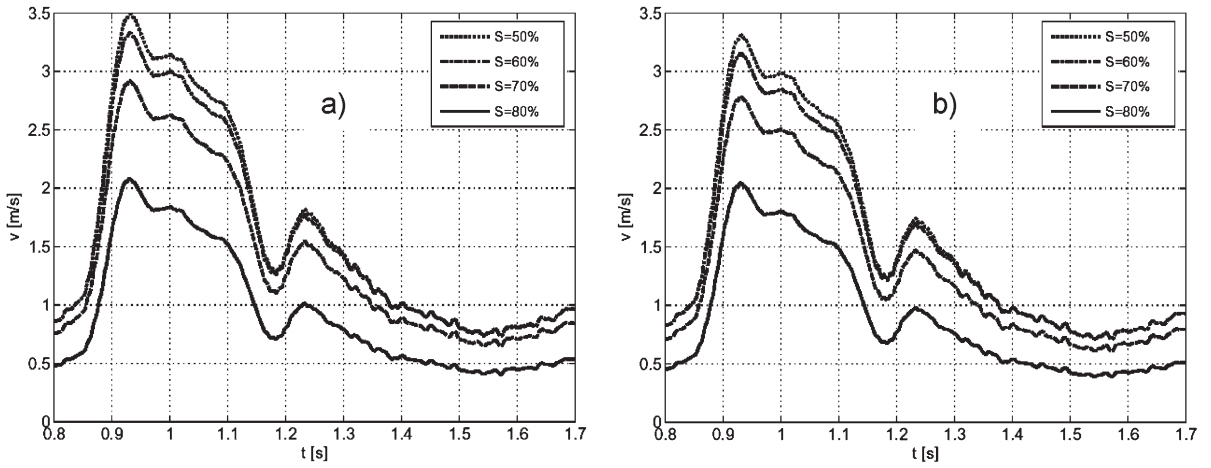

Fig. 4. Mean velocity at throat versus time with FSI: a) symmetric stenotic arteries, b) non-symmetric stenotic arteries.

Table 3
Maximal WSS (located at throat) and minimal pressure (located at throat) for systolic time 0.932 s with FSI

	WSS max [Pa]		*P* min [Pa]	
S [%]	Sym	Non-sym	Sym	Non-sym
50	1553.	1460.	−1977.	−1622.
60	1533.	1674.	−3190.	−2935.
70	1684.	1709.	−3509.	−2815.
80	1726.	1759.	−1488.	−1789.

systolic time 0.932 s. Between the two finer grid sizes the predictions of mean velocity are similar, so that we use a grid density with around of 500 tetrahedral elements/mm^3 in the fluid for the simulation with FSI in our stenotic artery models.

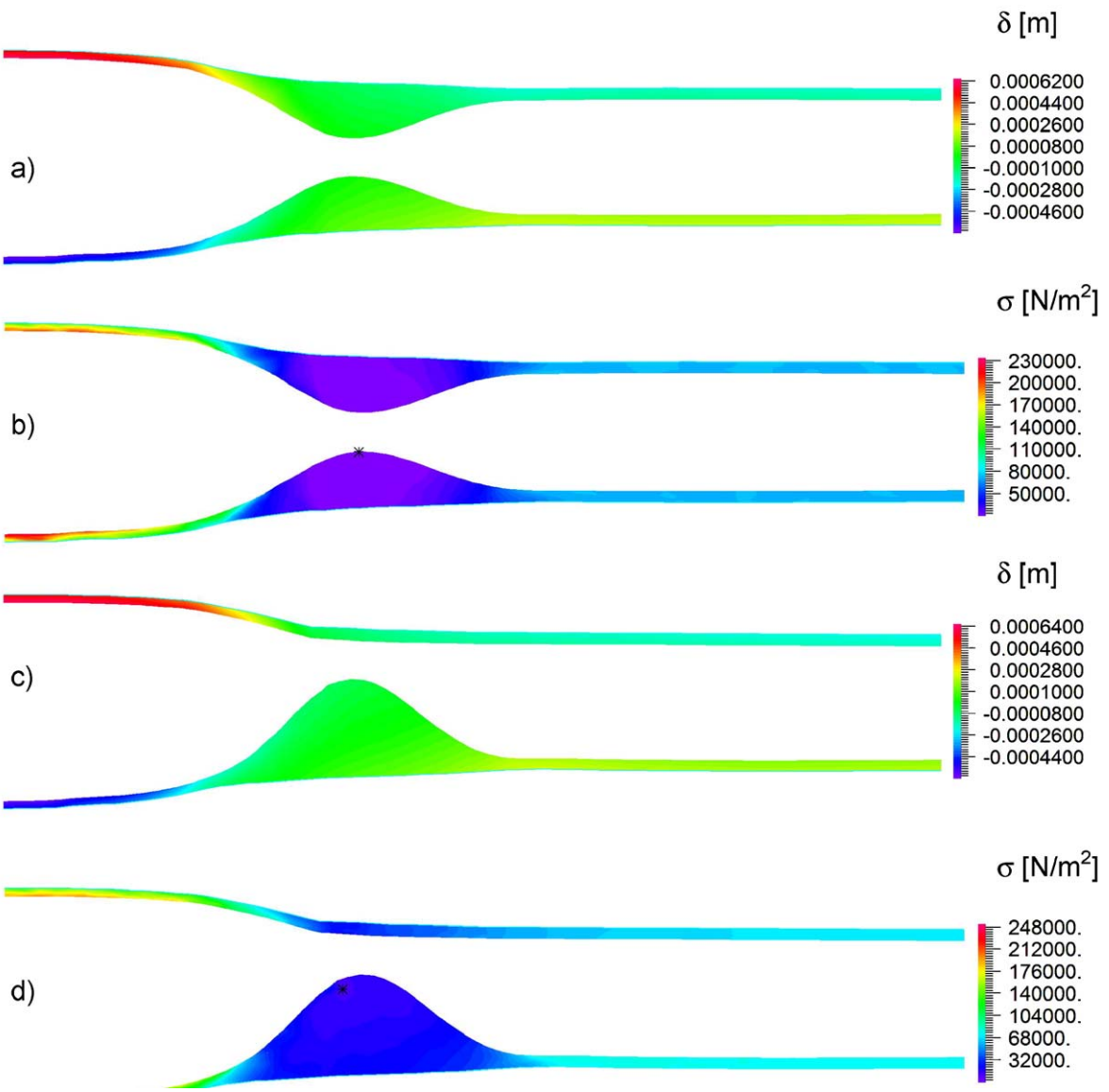

Fig. 5. a) Wall displacement for the symmetric stenotic artery, b) effective wall stress for the symmetric stenotic artery, c) Wall displacement for the non-symmetric stenotic artery, d) effective wall stress for the non-symmetric stenotic artery. Cases with S=70%, values at systolic time 0.932 s.

The workstation used to perform the simulations in this work is based on an Intel Pentium IV processor of 3.2 Ghz clock speed, 2.0 Gb RAM memory, and running on Microsoft Windows XP operating system. The simulation time for one FSI case based on 2 consecutive pulsatile flow cycles employing 857 time iterations was approximately 200 CPU h.

3. Results and discussion

The time dependence of mean velocity at throat for the symmetric and non-symmetric stenotic arteries modeled with rigid walls and inlet velocity boundary condition are shown in Fig. 3. The velocity increases in non-linear form with the stenosis severity and the symmetric stenosis produces higher mean velocity at throat as the non-symmetric stenosis. The maximal pressure (at inlet) and the minimal pressure (at throat) for systolic time 0.932 s, for the symmetric and non-symmetric stenosis are shown in Table 2. For symmetric stenosis with $S=80\%$ the maximal mean velocity is 20 m/s with a maximal pressure of 3.5×10^5 Pa. These values are not realistic from a physiological point of view, and therefore these cases are not representative for the flow in cerebral arteries.

The time dependence of mean velocity at throat for the symmetric and non-symmetric stenotic arteries modeled with FSI and inlet pressure boundary condition are shown in Fig. 4. The velocity decreases in non-linear form with the stenosis severity and with $S=80\%$ and 70% the symmetric and non-symmetric stenosis produce similar variation of mean velocity with time. The maximal WSS at throat and the minimal pressure at throat for the symmetric and non-symmetric stenosis are shown in Table 3. The maximal

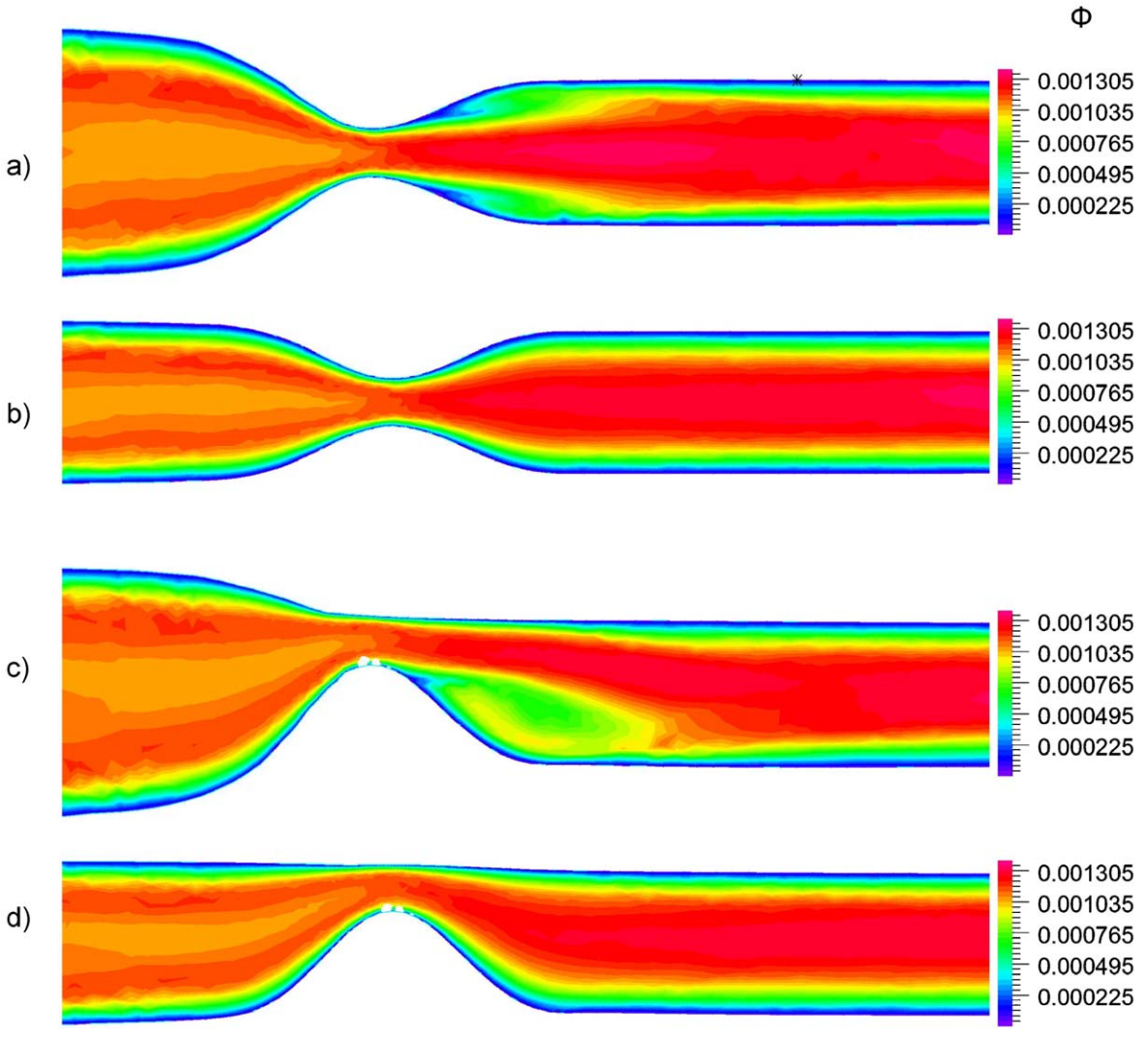

Fig. 6. Distribution of LDL concentration in stenotic arteries with FSI and for $S=70\%$, a) symmetric model, systolic time 0.932 s, b) symmetric model, diastolic time 1.548 s, c) non-symmetric model, systolic time 0.932 s, b) non-symmetric model, diastolic time 1.548 s.

Table 4
Instantaneous recirculation length at systolic time 0.932 s

	Lr [mm] rigid artery		Lr [mm] FSI	
S [%]	Sym	Non-sym	Sym	Non-sym
50	0	4.91	2.60	4.59
60	7.52	7.04	3.43	4.69
70	13.6	8.67	2.83	3.64
80	24.8	10.2	0	0

WSS for stenosis severity of $S=80\%$ are 1726. Pa and 1759. Pa for the symmetric and non-symmetric cases respectively, the corresponding values with rigid walls are 22,065. Pa and 36,000. Pa. For stenosis severity of $S=80\%$ the maximal mean velocity is 2 m/s with a pressure drop of 110 mm Hg. These values are realistic from a physiological point of view, and therefore these cases are representative for the flow in cerebral arteries.

The instantaneous recirculation lengths at systolic time for the eight cases simulated with rigid walls and velocity inlet and for the eight cases simulated with FSI and pressure inlet are shown in Table 4. With velocity inlet the recirculation length increases with S, however for the cases simulated with pressure inlet the recirculation length decreases with S. For $S=80\%$ and pressure inlet boundary condition the flow of diseases blood does not show recirculation zone after the stenosis.

The arterial wall displacement and effective wall stress for the symmetric stenosis and non-symmetric stenosis are shown in Fig. 5 for the cases with $S=70\%$ at systolic time 0.932 s. The maximal displacement is around a factor 2.6 and the maximal compression is a factor 1.8 of arterial thickness respectively. The maximum and minimum artery diameter at inlet are 3,4 mm and 2.3 mm at systolic and diastolic times respectively. The breaking strength of a normal cerebral artery is around 1 MPa, the maximal effective stress at systolic time is around 25% of the breaking strength of the artery. At stenosis throat the effective stress is very low.

The distribution of concentration of LDL changes over one cardiac cycle due the dilatation and compression of the artery. Fig. 6 shows the concentration of LDL for the symmetric and for the non-symmetric stenotic arteries for $S=70\%$ at systolic time 0.932 s and diastolic time 1.548 s. At systolic time the recirculation zone after the stenosis can be observed, and at diastolic time the flow after the stenosis does not exhibits separation of the wall, therefore the concentration of LDL and the related mass transfer on the artery wall changes due the stenosis over one cardiac cycle. Due to the artery compression downstream the stenosis the LDL concentration is greater than the inlet concentration.

4. Conclusions

This work presents a numerical investigation on the fluid-structure interaction of eight stenotic artery models, also the respective eight stenotic artery models with rigid walls are simulated for comparison. The effects of the inlet boundary condition are studied in detail. The inlet boundary condition of pressure is critical to obtain realistic hemodynamic results in stenotic arteries with diseases blood condition. The model of stenotic artery with rigid walls is not realistic, because the artery is considerably dilated and compressed in one cardiac cycle. The geometry and severity of the stenosis have effects on recirculation length, wall displacement, effective wall stress, and distribution of LDL concentration.

Acknowledgments

The financial support received from FONDECYT Chile under grant number 1030679 is recognized and appreciated. We thank Dr. Marcelo Galvez from the Instituto de Neurocirugia. Dr. Asenjo for providing the motivation and the material used in this work.

References

[1] J. Stroud, S. Berger, D. Saloner, Influence of stenosis morphology on flow through severely stenotic vessels: implications for plaque rupture, Journal of Biomechanics 33 (2000) 443–455.
[2] W. Liao, T. Lee, H. Low, Numerical studies of physiological pulsatile flow through constricted tube, International Journal of Numerical Methods for Heat & Fluid Flow 14 (2004) 689–713.
[3] D. Bluestein, C. Gutierrez, M. Londono, M. Schoephoerster, Vortex shedding in steady flow through a model of an arterial stenosis and its relevance to mural platelet deposition, Annals of Biomedical Engineering 27 (1999) 763–773.

[4] M. Bathe, R.D. Kamm, A fluid-structure interaction finite element analysis of pulsatile blood flow through a compliant stenotic artery, ASME Journal of Biomechanical Engineering 121 (1999) 361–369.
[5] D. Tang, C. Yang, H. Walker, S. Kobayashi, D. Ku, Simulating cyclic artery compression using a 3D unsteady model with fluid-structure interactions, Computers and Structures 80 (2002) 1651–1665.
[6] D. Tang, C. Yang, S. Kobayashi, D. Ku, Effect of a lipid pool on stress/strain distributions in stenotic arteries: 3D fluid-structure (FSI) models, Journal of Biomechanical Engineering 126 (2004) 363–370.
[7] D. Tang, C. Yang, J. Zheng, P. Woodard, G. Sicard, J. Saffitz, C. Yuang, 3D MRI-based multicomponent FSI models for atherosclerotic plaques, Annals of Biomedical Engineering 32 (2004) 947–960.
[8] T.K. Hsiai, S.K. Cho, H.M. Honda, S. Hama, M. Navab, L.L. Demer, C.M. Ho, Endothelial cell dynamics under pulsating flows: Significance of high versus low shear stress slew rates ($\partial\tau/\partial t$), Annals of Biomedical Engineering 30 (2002) 646–656.
[9] J. Stroud, S. Berger, D. Saloner, Numerical analysis of flow through a severely stenotic carotid artery bifurcation, Journal of Biomechanical Engineering 124 (2002) 9–20.
[10] S. Varghese, S. Frankel, Numerical modeling of pulsatile turbulent flow in stenotic vessels, Journal of Biomechanical Engineering 125 (2003) 445–460.
[11] D. Stangeby, C. Ethier, Computational analysis of coupled blood-wall arterial LDL transport, ASME Journal of Biomechanical Engineering 124 (2002) 1–8.
[12] M. Kaazempur-Mofrad, S. Wada, J. Myers, C. Ethier, Mass transport and fluid flow in stenotic arteries: axisymmetric and asymmetric models, International Journal of Heat and Mass Transfer 48 (2005) 4510–4517.
[13] M. Mannik, Blood viscosity in Waldenström's Macroglobulinemia, Blood 44 (1974) 87–98.
[14] B. Johnston, P. Johnston, S. Corney, D. Kilpatrick, Non-Newtonian blood flow in human coronary arteries: steady state simulations, Journal of Biomechanics 37 (2004) 709–720.
[15] S.F. Tsai, T.W. Sheu, Finite-element analysis of incompressible Navier–Stokes equations involving exit pressure boundary conditions, Numerical Heat Transfer. Part B, Fundamentals 39 (2001) 479–507.
[16] ADINA Theory and Modeling Guide, Volume I: ADINA, ADINA R&D Inc., Watertown, MA, USA, 2004.